Laser and Particle Beams (2003), *21*, 109–113. Printed in the USA.

DOI: 10.1017/S0263034603211204

Kinetic simulation of the coherent radio emission from pulsars

RÜDIGER SCHOPPER,[1] HARTMUT RUHL,[2] THOMAS A. KUNZL,[3] AND HARALD LESCH[1]

[1]Universitäts-Sternwarte München, München, Germany
[2]General Atomics, San Diego, California
[3]Max Planck Institut für Quantenoptik, Garching, Germany

(RECEIVED 13 March 2003; ACCEPTED 15 April 2003)

Abstract

On hand of 3D PIC simulations we show that in a strongly magnetized plasma a relativistic electron beam can be forced to emit highly coherent radio emission by self-induced nonlinear density fluctuations. Such slowly moving nonlinear structures oscillate with the local plasma frequency at which the relativistic electrons are scattered. Beam electrons dissipate a significant amount of their kinetic energy by inverse Compton radiation at a frequency of about $\gamma^2\omega_{pe}$. Since the beam is sliced into pancake structures which experience the same electric field the inverse Compton scattering is coherent. Such a process is a very promising candidate for the coherent radio emission of pulsars.

Neutron stars represent the most exotic state of matter with the highest densities accessible for direct observations in the universe. A subclass of neutron stars are sources of pulsating radio emission—the so called pulsars. Pulsars are fast rotating neutron stars (radius $r_{NS} = 10$ km, rotation periods $P \simeq 10^{-3} - 10$ s) with super strong surface magnetic fields of $B_0 \simeq 10^8$ T and an induced quadrupolar electric field of 10^{12} V/m which extracts particles out of the neutron star surface. This gives a density $n_{gj} = 10^{18}$ m^{-3} $(B_0/10^8\text{T})(P/\text{s})^{-1}$, which exactly cancels the parallel electric field components and forces the magnetosphere to corotate rigidly with the neutron star up to the so called light cylinder $R_L = cP/2\pi$. The typical distances of pulsars from the Earth is a few thousand light years but their pulsed radio emission is still so intense that the pulse structure can be investigated down to some 10 nanoseconds (Hankins, 1995). There seems to exist a radiation mechanism which allows a clear identification of a few meter sized emission region on distances of 10^{19} meters! Such super-intense radio emission can only be produced by a coherent radiation process, in which about 10^{15-17} particles radiate like one super emitter (Melrose, 2000). Thirty five years after its first detection the phenomenon of super-intense radio emission from pulsars still waits for a convincing explanation, especially the process which forces so many particles to radiate in a coherent way is not known. In this contribution we present particle in cell simulations of the plasma in the magnetosphere of a neutron star which show for the first time the bunching mechanism which may be responsible for the coherent emission in the radio frequency range.

Our model enables us to investigate the consequences of the non stationary particle extraction from the neutron star surface (Usov, 1987). Let us consider two subsequent discharges at the magnetic poles of the rotating neutron star: A first generation of particles is extracted up to the density n_{gj} which shields the electric field only for some unspecified time interval. This first generation then moves along the rotating strong magnetic field toward the light cylinder and loose energy due to the coherent radiation mechanism. In the meantime a second generation of particles is expelled from the neutron star, also moves toward the light cylinder and encounters the lower energy particles which leads to a two-stream-instability that is well-known to be a very efficient source for strong density fluctuations (Berk & Roberts, 1967; Morse & Nielson, 1969). In what follows we consider the low energy population as the background plasma and the high energy component as the beam (REB).

In a strongly magnetized plasma such density oscillations are predominantly longitudinal Langmuir waves oscillating with the plasma frequency $\omega_{pe} = \sqrt{ne^2/(\varepsilon_0 m_e)}$ which grow to nonlinear amplitudes (Kato *et al*., 1983; Weatherall, 1988; Benford & Weatherall, 1991). This instability can be ana-

Address correspondence and reprint requests to: Rüdiger Schopper, Max Planck Institut für Extraterrestrische Physik, PO Box 1312, Garching 85741, Germany. E-mail: schopper@usm.uni-muenchen.de.

lytically investigated only in its linear regime where the density fluctuations are supposed to be weaker than the undisturbed density. Its linear growth rate is given by (Melrose & Gedalin, 1999): $\Gamma_{\rm lin} \simeq \omega_{\rm pe}/\gamma_{\rm b}\langle\gamma_{\rm e}\rangle$, where $\gamma_{\rm e/b}$ denotes the Lorentz factor of the background/beam electrons. The interaction of the REB with the electrostatic fluctuations of the Langmuir waves results in very strong coherent electromagnetic waves (Kato *et al.*, 1983; Levron *et al.*, 1987). In the rest frame of the beam electrons, they experience the Doppler shifted electrostatic wave with $\omega \simeq \omega_{\rm pe}$ moving towards them with the Lorentz factor γ. The nonlinear interaction with the waves force the REB to wiggle and to emit dipole radiation of the same frequency as the waves, that is, $\gamma\omega_{\rm pe}$. In the laboratory frame this Hertz' dipole radiation is again Doppler boosted and strongly beamed in forward direction due to the relativistic lighthouse effect. Thus the observer measures the frequency $\gamma^2\omega_{\rm pe}$. This interaction can be interpreted as coherent inverse Compton scattering (CICS) of Langmuir waves (Benford & Weatherall, 1988). Coherence would occur due to the bunch structure of the beam which means a phase coupled electrostatic field and density modulation.

Radio observations indicate that at about 100 pulsar radii from the strongly magnetized neutron star the coherent pulsed radio emission is produced (Kunzl *et al.*, 1998; Melrose *et al.*, 1999; Melrose, 2000; Kijak, 2001). Due to the dipolar magnetic field structure the shielding density $n_{\rm gj}$ drops as $(r/r_{\rm NS})^{-3}$, that is, at 100 pulsar radii its value is $n_{\rm e} = n_{\rm b} = 10^{12}\,{\rm m}^{-3}$, which is equal for the beam and the plasma, which corresponds to a plasma frequency of $5.6\cdot10^7\,{\rm s}^{-1}$. From the condition that the emitted frequency must be larger than the plasma frequency (Kunzl, 1998) the beam electron Lorenz factor was chosen to be $\gamma = \sqrt{5}\,(\gamma\beta = 2)$. The magnetic field at 100 pulsar radii is still very strong namely about 1000 T (Pacini, 1967).

Especially the strong guiding field is important for the efficiency of the CICS-process. It reduces the electron dynamics to the spatial dimension along the magnetic field lines which greatly improves the stability of the excited Langmuir waves and thus leads to strong and stable electrostatic wiggler fields (Pelletier *et al.*, 1988). For the temperature of both the beam- and background electrons we take the value derived from X-ray observations (Pavlov & Petekhin, 1995) of $T_{\rm e} = T_{\rm b} = 100$ eV as typical polar cap temperature of neutron stars. The PIC-code used for this numerical simulation is fully three dimensional and it conserves mass and energy (Ruhl, 2000). In the simulation the direction of electron beam propagation $\gamma\beta$ and of the magnetic field $\boldsymbol{B}$ is the positive z-direction, which is also called the longitudinal direction. The simulated box has a numerical extension of $80 \times 80 \times 200$ grid points and a physical extension of 100 m $\times$ 100 m $\times$ 250 m, which corresponds to the size of the expected features. The resolution of $\delta x = \delta y = \delta z = 1.25$ m is more than sufficient to resolve the expected minimum wavelengths of approximately $\lambda_{\rm Rad} = 2\pi/k_{\rm Rad} = 2\pi c/\gamma^2\omega_{\rm pe} \approx 6.7$ m. A particle density of $10^{12}\,{\rm m}^{-3}$ is approximated by 10 quasi particles per cell, leading to 16 million background quasi electrons that are accompanied by a varying number of beam quasi electrons of not more than 2.5 million, which eventually enter the computational box. Those numbers are doubled, since for quasi neutrality an equally large number of positive particles are required.

The initial condition is given by a homogeneous background plasma of density $n_{\rm e}$, temperature $T_{\rm e}$ and a longitudinal magnetic field $B_z = 0.1$ T. This too low value, which significantly simplifies numerics, is found to be sufficiently high to represent a much stronger field of 1000 T ($\omega_{\rm ce} \gg \omega_{\rm pe}$). Initially there is no beam in the computational box. The beam is injected later at the $z = 0$ plane of the box with a density profile of $n(r) = n_{\rm b}/(1 + \exp[(r - R)/\Delta R])$. Here r denotes the distance from the x-y center of the box and $R =$ 20 m and $\Delta R = 3$ m give the radius and the sharpness of the electron beam. The homogeneous background plasma is disturbed in phase space (see Fig. 1) in order to accelerate the excitation of Langmuir waves by giving the system a hint of the relevant length scales. We used the wave length of the fastest growing Langmuir mode, which follows from an analytic calculation of the linear growth rate $\Gamma_{\rm lin}$. The disturbance is chosen not to induce any finite charge or current densities, thus leaving the background plasma initially homogeneous, neutral, and current free.

The boundary conditions during the simulation are quite simple. In the transversal directions x and y we chose periodic boundaries and in the longitudinal direction z the box is open, which means that plasma particles and fields can leave the box unaffected. In addition at the lower z plane ($z = 0$) an electron component is continuously injected with the density profile mentioned above, a mean $\gamma\beta$ of 2 and the temperature $T_{\rm b}$.

The simulation runs for 600 time steps with $\delta t = 2.41$ ns. The total time simulated was 1.44 μs, after which the growing nonlinear Langmur waves saturate and a quasi stationary situation had developed as it is shown in the next section.

The beam particles entering the computational box interact with the faint traces of fluctuations we introduced in or

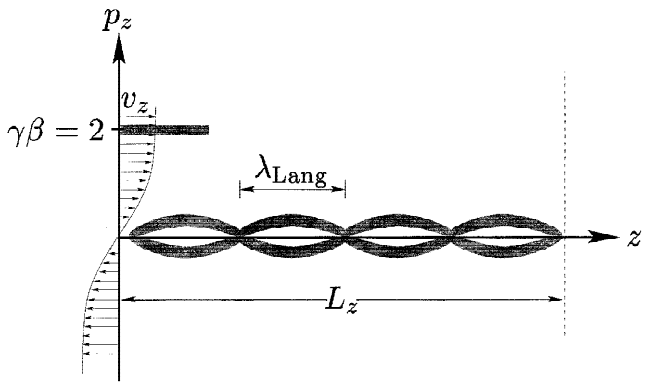

Fig. 1. The initial configuration of electron phase space including the beam. The initial disturbance of the background plasma is heavily exaggerated for reasons of better display.

https://doi.org/10.1017/S0263034603211204 Published online by Cambridge University Press

initial setup and excite the appropriate modes to grow. In Figure 2 the phase space of the electrons in z-direction after 400 time steps is presented. In this plot the fully developed Langmuir turbulence is visible. After 962 ns, the disturbance in the beam and the background has grown so strong, that both components start to mix, that is, there is no distinction between beam and background electrons anymore. Beam electrons are strongly decelerated even until $v \simeq 0$, whereas background electrons are accelerated up to a Lorenz factor of 5. The extremely strong accelerations are due to the strong electrostatic fields of the excited Langmuir waves. Since the Langmuir turbulence structure in Figure 2 moves with a much lower speed (which is even continuously decreasing throughout the simulation) than the yet unaffected beam electrons, it acts as the wiggler field that stimulates the CICS-emission. The electrostatic fluctuations directly correspond to electron density fluctuations (solid curve in Fig. 2), which reach a value of $\sim +100\%/-50\%$ oriented at $n = n_\mathrm{e} + n_\mathrm{b} = 2{\cdot}10^{12}\ \mathrm{m}^{-3}$. The structure of the electron density is better seen in Figure 3, where the contour surface at $n = 1.5{\cdot}10^{12}\ \mathrm{m}^{-3}$ and a cut through the electron beam is shown. The electron density varies between 4 and 1 times $10^{12}\ \mathrm{m}^{-3}$, which implies the strong electrostatic fields. It can be clearly seen, that the beam decays in a series of "pancakes". Such pancakes are absolutely necessary to explain the coherent nature of the pulsed radio emission of neutron stars. Since the emission from relativistic particles is confined to a forward cone with half angle $\sim 1/\gamma$ and the emission is nearly along the magnetic field. Thus, in Fourier space bunching emission corresponds to the component $k_\perp$ to the fields being smaller than the component $k_\parallel$ along the field line by a factor $1/\gamma$. This corresponds to flat pancake shaped bunch with the normal within an angle $1/\gamma$ of B (Melrose, 2000). This is exactly what we observe in our simulations! We briefly note that our simulations are the first ones which

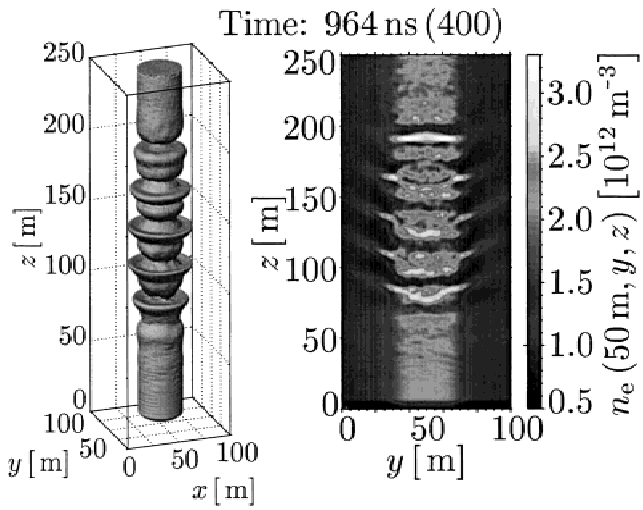

Fig. 3. 3D electron density contour surface (left) and the profile of the electron density (right) after 400 time steps. In the right plot a cut through the center (x = 50 m) of the electron beam has been made. The color represents the value of the electron density at a given point.

show this kind of pancake bunches! The number of particles in such a pancake corresponds to the maximum coherence achievable for CICS and it should be noted, that in our simulation the thickness of such a pancake is significantly larger ($\gtrsim 1$ m) than the Debye length which is usually used in analytical models (Kato *et al.*, 1983; Levron *et al.*, 1987; Weatherall 1998). A typical volume of one bunch is about 10 m^3 giving a total number of particles per bunch of about 10^{13}. Our simulations prove, that a much higher coherence is achievable than expected from analytical models.

The growth of Langmuir waves can be deduced by the Fourier transform of the electrostatic field $\tilde{E}_z$. In Figure 4 the energy density of the electrostatic modes is plotted versus the corresponding wavenumber k and time t. The

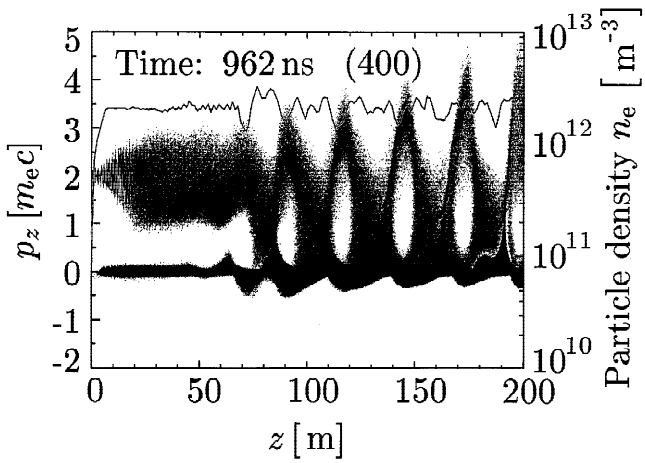

Fig. 2. Electron phase space in z-direction after 400 time steps (962 ns). The quasi particles are plotted as dots according to their corresponding position in z (ordinate) and their momentum p_z (left abscissa). The curve presents the particle density of the electrons (right abscissa).

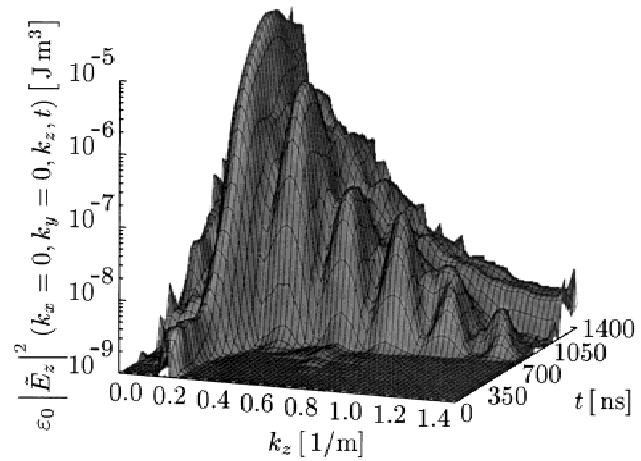

Fig. 4. The electrostatic mode energy density is plotted against wave number k and time t. The linear growth rate for the fastest growing mode is given by $\Gamma_\mathrm{lin} = 2{\cdot}10^{-2}\ \mathrm{ns}^{-1}$.

https://doi.org/10.1017/S0263034603211204 Published online by Cambridge University Press

$k \simeq 0.25\ \mathrm{m}^{-1}$ mode is growing by four orders of magnitudes within some ten nanoseconds. It should be noted however, that the fastest growing mode ($k = 0.25\ \mathrm{m}^{-1}$) is slightly off compared to the initially given wave number ($k_{\max} = 0.21\ \mathrm{m}^{-1}$, where $k_{\max}$ corresponds to the maximum of the imaginary part of ω in $1 = 1/k^2 \int [(\mathrm{d}v/\mathrm{d}p)/(v - (\omega/k))^2]\, f \mathrm{d}p$), which can be seen in Figure 4 as the small peak at early times. This means, that for our simulation the analytical value for the fastest growing mode is not precisely correct and it proves, that although the initial disturbance has given a hint to the system it has not forced it toward an unphysical solution. We note that the wave energy density is distributed to higher k when it exceeds a value of about 10^{-7} J m^3, driven by nonlinear wave–wave interactions.

We emphasize that the strong wave-particle interaction which drives the bunching is self-consistently excited along the propagation direction of the beam. The strongest emission originates in regions with the largest density gradients (Fig. 5). Every deceleration and acceleration region forces the beam electrons to emit Hertz' dipole radiation, which is beamed in forward direction, as can be seen in Figure 6 (right). θ_{M} represents the angle of maximum intensity, expected from theoretical consideration ($\tan \theta_{\mathrm{M}} = 1/2\gamma\beta$) with a $\gamma\beta = 2$. The striking resemblance with a relativistically beamed Hertz' dipole is obvious, but the emission characteristic in our simulation also gives precisely the expected opening angle of the emission cone, which is proposed for a CICS-process. In Figure 6 (left) the "spectrum" of the emitted radiation is shown, which has a strong peak at $\omega = 5\omega_{\mathrm{pe}}$ and a couple of minor peaks at $4\omega_{\mathrm{pe}}$ and $3\omega_{\mathrm{pe}}$ due to nonlinear wave coupling and beating between electromagnetic and electrostatic waves. Again we find rather precisely the theoretically expected value of $\omega = \gamma^2\omega_{\mathrm{pe}}$. The total power emitted by the simulated computational box is shown in Figure 7. It is the escaping Poynting flux at the top of the computational box ($z = 250$ m) integrated over the top surface. After about 850 ns the emitted power rises within some ten nanoseconds by more than 6 orders of magnitude to a value of 1 GW. Afterward the total output power increases more slowly by one more order of magnitude and reaches a maximum of 10 GW continuous radiative power at the end of the simulation. This is a significant fraction of the power injected by kinetic energy of the beam particles, shown in Figure 7 as + symbols at a constant value of 50 GW. The rest of the energy leaves the box as kinetic energy of beam electrons, which would probably be also emitted if the computational box would have a greater size in z-direction.

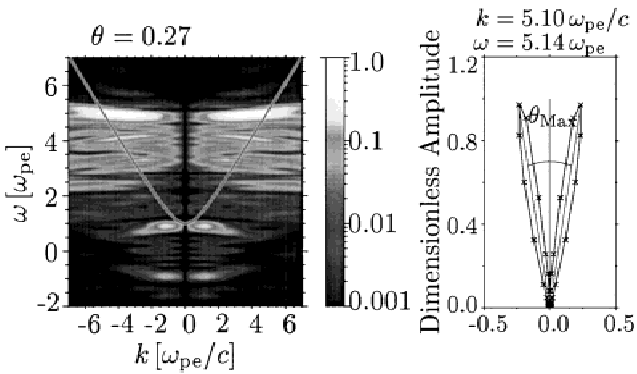

Fig. 6. Dispersion relation (left) and emission characteristic (right) of the emitted radiation. For the left plot the angle θ_{M}, the angle of maximum intensity, has been used. The curve in the left plot gives a hint to one of the propagating dispersion branches of electromagnetic radiation. We note that for our parameters the dispersion branch is very close to the freely propagating branch of Appleton-Hartree dispersion relation for oblique propagating electromagnetic waves in strongly magnetized plasmas. The right diagram presents the intensity of the radiation for a given θ in a polar plot. θ is the angle between beam direction and direction of emission. The values in both diagrams are normalized to a value of one.

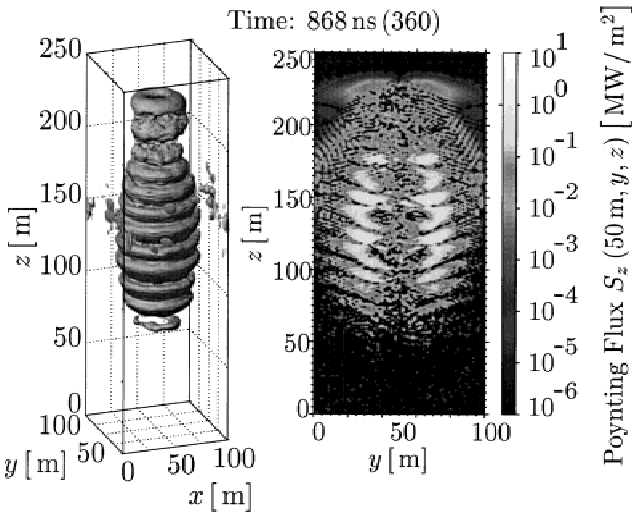

Fig. 5. Structure of the emitted Poynting flux as 3D contour surface of the value $2.5 \cdot 10^4$ W/m^2 (left) and as a cut through the center of the beam at $x = 50$ m (right).

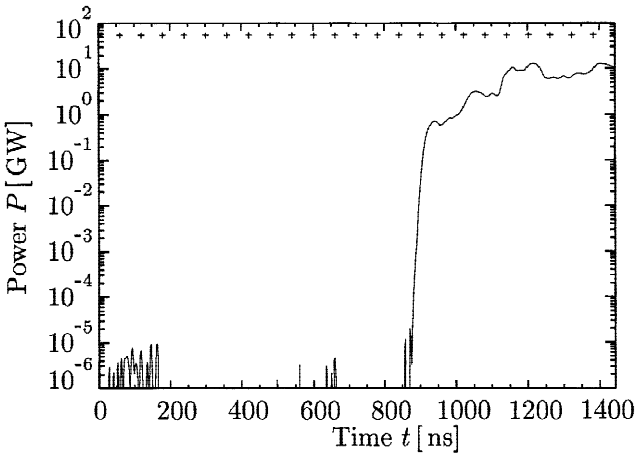

Fig. 7. The output power injected by kinetic energy of the beam particles increases more slowly, as shown by a + symbol, at a constant value of 50 GW.

https://doi.org/10.1017/S0263034603211204 Published online by Cambridge University Press

ACKNOWLEDGMENTS

The authors would like to thank the John von Neumann Institute for Computing (NIC) and the Leibniz Rechenzentrum München for the granted computational time and the Deutsche Forschungsgemeinschaft which supported our work through the grant LE 1039/3-1.

REFERENCES

Benford, G. & Weatherall, J.C. (1991). *APJ* **378**, 543.
Berk, H.I. & Roberts, K.V. (1967). *PRL* **19**, 297.
Hankins, T. (1995). *APJ* **453**, 433.
Kato, K. *et al.* (1983). *Phys. Fluids* **26**, 3636.
Kijak, J. (2001). *MNRAS* **323**, 573.
Kunzl, T.A. *et al.* (1998). *APJ* **505**, L139.
Levron, P., Benford, G., & Tzach, D. (1987). *PRL* **58**, 1336.
Melrose, D.B. (2000). In *Pulsar Astronomy*.
Melrose, D.B. & Gedalin, M. (1999). *APJ* **505**, 351.
Morse, R.L. & Nielson, C.W. (1969). *PRL* **23**, 1087.
Pacini, F. (1967). *Nature* **216**, 567.
Pavlov, G.G. & Petekhin, A.Y. (1995). *APJ* **450**, 883.
Pelletier, G. *et al.* (1998). *Phys. Rev. A* **38**, 2552.
Ruhl, H. (2000). Habilitation Thesis, TU-Darmstadt.
Usov, V.V. (1987). *APJ* **320**, 333.
Weatherall, J.C. (1998). *PRL* **60**, 1302.